

C.O.L. Hamilton Smith^{1,2} & N.J. Lawson¹

¹School of Aerospace, Mechanical and Mechatronic Engineering University of Sydney ²DMTC Limited, Level 1 620 High St, Kew VIC 3101

Abstract

Wind-tunnel (WT) tests were conducted with hot-wire anemometry (HWA) to map the boundary layer (BL) prior to an open-narrow cavity of L/D=L/W=3, at $U_\infty=10\text{-}20\text{m/s}$, for comparison to the BL in absence of the cavity. Changes in upstream (U/S) geometry via fuselage and nose curvature were also used to alter the BL profile, and observe the impact on cavity response in comparison to a flat-plate baseline, with and without the cavity. Cavity response was indicated by internal unsteady surface pressure (USP) measurements. Results highlight a measurable change in BL profile when a cavity is present, compared to when absent, in all cases. BL profile also changed for each U/S geometry, prior to the cavity, altering internal cavity response, in all cases. This finding of a thin BL returning more energetic cavity excitation is consistent with the literature, in contrast to a thick BL, which attenuates the cavity response. These findings hence highlight the impact of altered U/S geometry from a flat-plate, and it's effect on the BL. They also show initial flat-plate BL disturbance thickness δ , must also be considered in conjunction with turbulence intensity (TI), displacement δ^* and momentum thickness θ , for a full picture of flow response, as the cavity impacts the U/S BL structure in the presence of feedback. This work is part of a larger study, aiming to discretise BL phenomena with respect to; TI, δ , δ^* and θ , and how each is manipulated by geometry, in the presence of a cavity down-stream (D/S), for prediction of cavity spectral response and feedback.

Keywords: Cavity Flow, Aerodynamics, Boundary-Layer, Turbulence, Momentum

1. Introduction

Cavity flow has been extensively studied in it's most detrimental forms; landing gear and bomb bays, with effects of; increased drag leading to higher fuel consumption, noise resulting in instrument interference, and structural fatigue. Research has covered a large range of Mach M_{∞} and geometry to understand, model and control the flow. However, limited work has covered the BL effect, and how it couples to the flow. Nonetheless, literature observant of the U/S BL $^{[1-6]}$, has highlighted the importance of mapping its flow structures prior to the cavity, as they provide valuable insight into the phenomena. In the following paper, HWA has been used to identify, map and correlate the U/S BL profile and how it changes in the presence of a cavity, and in response to varied U/S geometry. Further work, will use this analysis to distinguish U/S flow structures in the cavity response, and cavity feedback structures in the U/S BL itself, with potential to correlate change in temporal flow input, and update real-time data toward more accurate prediction of cavity flow.

1.1 Cavity Flow Phenomena

Cavity flow at subsonic Mach numbers have aero-acoustic feedback mechanisms, with high intensity vortical structures, capturing large self-sustained pressure oscillations (SSOs), fluctuating in the bounds of and interacting with a shear layer (SL) per Figure 1. Form, magnitude, and location are determined by how the U/S BL separates into a SL, which impinges at a certain location in the cavity, dependant on internal geometry and momentum, defined by L/D, L/W, M_{∞} , δ and θ . Resonance can occur, with evidence at the cavity mouth suggesting associative dominance of SL instabilities. These structures form at BL separation, and convect D/S, further magnified by interaction with ideal

geometry, to form the feedback system responsible for dominant resonant tones. Mass exchange also occurs, as the SL expels energy on upward oscillation moving D/S, exchanging mass on downward oscillations, further exciting internal and SL instabilities. Overall, the SL, and how it forms and interacts with the cavity is most important. However, there is a lack of agreement on the SL formation from BL separation, with no agreed method to predict the entire spectral response given BL data, or the impact of cavity flow feedback U/S.

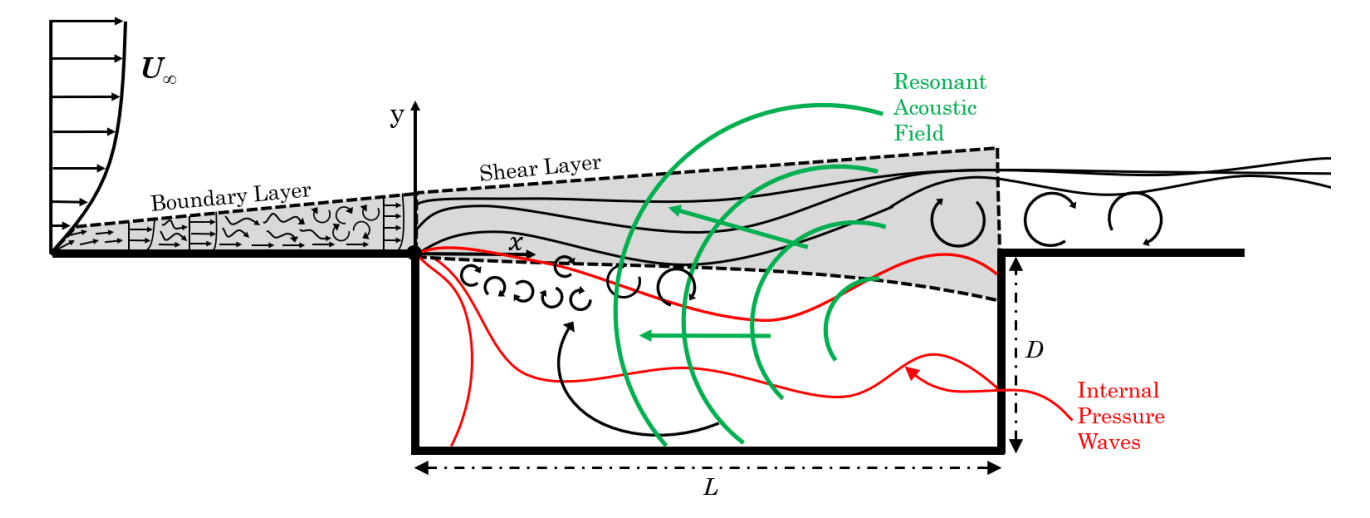


Figure 1 - The Cavity Flow Mechanism

Assuming uniform flow structure in all cavities is an oversight, as many parameters contribute to the SL and internal flow field. Even though similarities are shared, differences exist, which are dependant on geometry and U/S flow. Classification of; open, transitional and closed type flow, is dependant on how the SL interacts with cavity geometry. In closed (L/D>10), the SL sweeps inside attaching along the floor, separating again before the trailing edge (TE). In open (L/D<5), the SL bridges the cavity attaching near the TE. Transitional, is a region between where the SL appears to lean toward either with modality of both apparent modes. L/D is a requisite to define the flow type. However, U/S the BL can extend the boundaries, where a thick BL requires a longer cavity to establish open/resonant characteristics. In this case, the flow field tends towards closed less resonant response, but a thin BL tends towards open/resonant, proving the impact of U/S BL on cavity response. Similarly, a narrower cavity L/W>1, will tend toward closed compared to a wide geometry. It is known, irrespective of BL, characteristic pressure oscillations and acoustics can still occur. However magnitude with respect to noise and propagation differs significantly based on BL. This study observes turbulent BLs of varying shape, due to changes in U/S geometry; flat, parabolic, ogival and conic, concluding on evidence the U/S BL is a primary governing factor.

1.2 Review

Considering U/S BL effects on cavity flow, Karamcheti^[7] initially aligned a random buffet and weak resonant cavity response to a turbulent U/S BL, which is in contrast to a periodic pressure, and thus a distinct acoustic tonal response to a laminar U/S BL. It should be noted, a cavity subject to a turbulent U/S BL required larger L/D than a laminar U/S BL, at fixed M_{∞} and W, to establish periodicity for a resonant acoustic response. Roshko^[8] observed changes in modality and amplitude with increasing δ/D . Charwat et al^[9] also perceived change in the point of transition between open and closed flow or $(L/D)_{cr}$ as δ increased, almost independently of M_{∞} and Reynolds Number. Block & Heller^[10] proved the effectiveness of increasing δ to reduce noise. However effectiveness decreased with increased M_{∞} or L/D as flow transitioned open to closed, altering the noise mechanism from classic resonator to periodic, which is apparently less δ dependant.

Sarohia^[1] studied changes in laminar BLs on oscillatory cavity response, and amplified disturbances in the SL at low M_{∞} . Resulting cavity oscillations were observed to coerce large lateral SL motion close to the TE, causing periodic shedding of vortices from the TE at the same frequency. These

HOT-WIRE ANEMOMETRY OF THE BOUNDARY LAYER PRIOR TO A CAVITY IN RESPONSE TO VARIED

oscillations requiring a minimum length L_{min} , where for $\delta/D < 0.5$, if $L_{min}/\delta\sqrt{R_e\delta} < 290$, no oscillations occurred. Thus, increasing δ delayed oscillation onset, until a sharp increase at $L_{min}/\delta\sqrt{R_e\delta}$ for $\delta/D > 0.5$, where no oscillations occurred, and decreasing D stabilised SL laminarity. Thence, D appears to have little impact on oscillation when $\approx \delta$, due to a stabilising SL effect in response to the laminar BL. Strouhal Number N_{ST} was also found to be lower when subject to a turbulent BL compared to laminar, and transition to turbulent flow in the SL was postponed by an U/S laminar BL, in the presence of large amplitude periodic oscillations, until L_{min} where transition occurred.

Scheiman^[2] created a fully turbulent BL with vortex generators prior to a cavity, and aligned proportional tone attenuation alike [1; 7; 10]. Ahuja & Mendoza^[11] thickened the BL to eliminate noise, and aligned resultant attenuation to dispersion of the SL at $\delta/L \approx 0.07$. Further proven by control methods to physically disperse the SL to remove detrimental fluid phenomena, i.e., LE steady jet blowing, this thickened the BL, dispersing the SL, reducing tones^[11]. Colonius and Rowley et al^[12; 13] varied BL δ , and found laminar separation at the LE to be the cause of Wake Mode (WM), or high drag mode, due to resultant high pressure on the aft wall and low pressure on the fore. This caused by an increase in separation resistance, where a thick turbulent BL separated quicker, increasing pressure on the fore wall, and preventing oscillatory growth and convection into WM. Therefore, thickening the BL reduced tonal amplitude and drag. Milbank^[3] altered flow impingement location before a cavity to observe change in oscillatory response. They found a cavity closer to flow impingement, with a proportionally thinner BL, responded more periodically to local fluctuations than a cavity further D/S in a fully developed thick turbulent BL, which filtered tones and ceased transition to WM alike [12; 13].

Grace et al^[4] observed a laminar U/S BL to result in only a single internal vortex in their cavity, which was 31% stronger and closer to the TE, than produced by a turbulent U/S BL, with mean flow of negligible vertical velocity near the TE. The turbulent BL was of greater impact U/S, due to production of mean flow at the TE, moving U/S with a positive vertical velocity closer to the wall. Flow D/S was also found to converge on flat-plate turbulence at a slower rate, due to a turbulent BL U/S. The resultant random buffet delayed transition, whereas the more periodic laminar BL likened to the condition. This was further proven by Chang et al^[5], who studied the BL separation. Their laminar BL produced SL instabilities convecting streamwise. In this case, initial interaction with internal recirculation disturbed the LE shed spanwise vortices as they approached the TE, and were clipped into small hair-pin structures, convecting D/S aft the cavity. The turbulent BL had a broader spectrum with more recirculating flow U/S, and a strong normal velocity component, which produced SL buffet streamwise from incoming coherant structures. This effect influenced SL eddy formation. This resulted in convection as a randomised interaction, instead of the large spanwise structures formed by the laminar BL. Random buffet of the turbulent BL, also impacted mass exchange. For a laminar BL, with no random buffet, mass exchange was simultaneous between internal injection and external ejection via large scale spanwise vortices D/S. However, random buffet from the turbulent BL accelerated ejection, removing flow uniformity as the SL was perturbed U/S externally delaying flow injection in main recirculation.

Seena & Sung^[14] extracted DMD modes from an open cavity in response to a thick turbulent BL. They found no abundant oscillatory features, though BL structures were coincident in the viscous SL along the cavity mouth in frequency, but differing in wave number space. However, a thin BL produced large-scale structures from LE separation, resulting in formation of a fully coherent and structurally dominant dynamic peak. These peaks were aligned to the large oscillatory pressures of SSOs coincident with Rossiter Mode 3 in frequency and wave number space. Therefore, resonant SSOs only occur when the U/S BL and SL are coincident in frequency and wave space. Gharib & Roshko^[15] studied periodic SL SSOs and their relation to drag based on U/S BL. They identified the requirement for a thin BL to form SSOs, and high drag WM. For their conditions, SSOs only occurred when $L/\theta \ge 81$, below which the SL bridged and oscillations ceased, so $L/\theta = 81$ was the location of fundamental frequencies. Rossiter mode 2 was aligned to SSOs, where increasing L/θ decreased Mode 2 frequency, which then jumped to mode 3 dominance, and also decreased in frequency, until it was intermittent and disappeared. Thus a thin BL was required to develop SSOs, and mode switching occurred in the region between dominance, based on ratio L/θ .

HOT-WIRE ANEMOMETRY OF THE BOUNDARY LAYER PRIOR TO A CAVITY IN RESPONSE TO VARIED

Karamcheti^[16] studied thin and thick turbulent U/S BL effects, and perceived no SSOs or WM for $D/\theta < 15$. Over the threshold however, amplitude increased enabling recirculating flow to shift to absolute SL instability and form SSOs and then WM. Therefore, it was found a very thick BL decreases fluctuation amplitude inhibiting SSO formation and WM transition, reducing radiated acoustics by increasing L_{min} for oscillation. Haigermoser et al^[6] performed PIV on subsonic open flow with a very thick turbulent BL $L/\theta = 18$ and identified SSOs despite $L/\theta < 81$. However, they correlated irregular SL vortex shedding to similar coherant structures in the turbulent BL U/S, indicating dependence on the BL for SL instability. This agreed in theory with [15], but disagreed on the limit. Kang et al^[17] also disagreed on the limit, identifying statistically characterised SSO vortical structures in open cavity SLs in response to low M_{∞} and a thick turbulent BL $L/\theta < 81$. It must be noted, Gharib & Roshko [15] had an axisymmetric cavity of infinite-W, and Haigermoser et al [6] and Kang et al^[17] had a finite-W. Hence formation of SSOs, whilst dependant on BL as L/θ and δ/D , also dependant on W.

In summary, it is apparent cavity SL structure depends on U/S BL, with respect to the formation of coherant structures, modality and wave space. Further, a sufficiently thin BL is required in the LE vortex shedding, to form SSOs, WMs as a high drag mode, stable TE fluid mass exchange, and radiation of acoustic tones. Overall, U/S characteristics are primarily linked to cavity flow response, and must be considered as the nature and presence of fundamental flow features change.

2. Experimental Set-Up

HWA and USP were used to record flow data from the BL leading, up to and within a cavity, to assess how the BL is altered by varied U/S geometry, cavity presence, and the BLs impact on cavity response. Airspeed was $U_{\infty} = 10\text{-}20\text{m/s}$, which is $M_{\infty} = 0.03\text{-}0.06$. Ambient conditions are provided within the wind tunnel test matrix in the Appendix.

2.1 Wind Tunnel

The University of Sydney Closed-Circuit Low Speed Aerodynamics WT has an airspeed range of U_{∞} = 1-70m/s and BL $\delta \approx$ 39mm. Before the test section, air follows an octagonal cross-section with a bell mouth followed by a settling chamber of two screens. A contraction accelerates the flow into a (4 \times 3)ft test section. Due to the model's relative size and position in the WT, wall interference and blockage was calculated to be negligible, and no related corrections were therefore made. Airspeed is controlled by correlated fan RPM after the test-section, measured with pitot tubes U/S and D/S.

2.2 Cavity Model

A single cavity geometry was used, with four U/S geometries altering the BL prior to the cavity. These results were bench marked against the BL over the same U/S geometries with no cavity present, providing a total of eight HWA traverses. The cavity is open-narrow per L/D = L/W = 3, with L = 180mm and D = W = 60mm, within a $\varnothing 100$ mm cylinder emulating a fuselage. This body was mounted to the WT floor with a protrusion height of 84.4mm. Cylinder length was 505mm, including exchangeable U/S nose cones; conic, ogive and parabola, their centre above the WT BL. Cavity D in the fuselage varied spanwise with cylinder curvature, introducing additional effects, to show the impact of applied geometry, i.e., vehicle curves. This geometry was compared against a baseline flat cavity of the same L/D, L/W. Figure 2 is a schematic of the set-up.

2.3 Hot-Wire Anemometry

2.3.1 Mount Structure

The WT test-section had a removable roof, which was supplemented with a cut-out roof to insert the HWA probe. A translation stage was used to control probe location via an external mount, separated from the WT, to remove WT vibration. The mount was a \emptyset 12mm stainless steel rod, extending into the WT via the roof cut-out, with a small cut-out at the rod LE for the probe to sit. The probe had an interference fit, which was then secured with a lock-clip, and the steel rod was locked to the translation stage with a stainless steel lock-clip with a tight fit, to reduce vibration. Figure 3 shows the set-up.

2.3.2 Instrumentation and Acquisition

A Dantec Dynamics Streamline Pro was used, with; constant temperature anemometer (CTA), integrated measuring system interfaced to PC with an NI Daq A/D device, single-axis 90° probe, BL sensor, automatic-calibrator, and 3-axis traverse with an ISEL IMC-S8 Step Controller. The system enabled instantaneous measurement of fluid velocity to calculate statistical derivatives of; mean velocity U_M , turbulence intensity (TI), high order moments and spectra traversing points in space, with coincident pre and post calibration using polynomial derived constants. Each traverse moved through 30 logarithmically distributed points over 270mm in the Y-axis (vertical), to capture the Newtonian BL development at a constant point, centered U/S of cavity LE; X = -5mm, Z = 0mm, for all eight cases, totalling 240 points. A script was written to interface the CTA, A/D and PC, to record, and store data. The script established a connection, then looped through taking a measurement and moving Y-axis position, until all points were recorded, then increasing U_{∞} to repeat. Each measurement was taken for t = 60s at a rate of $SR = 2f_{max} = 2^{15}H_Z$ per Nyquist criterion, for $N = 1.97 \cdot 10^6$ samples,

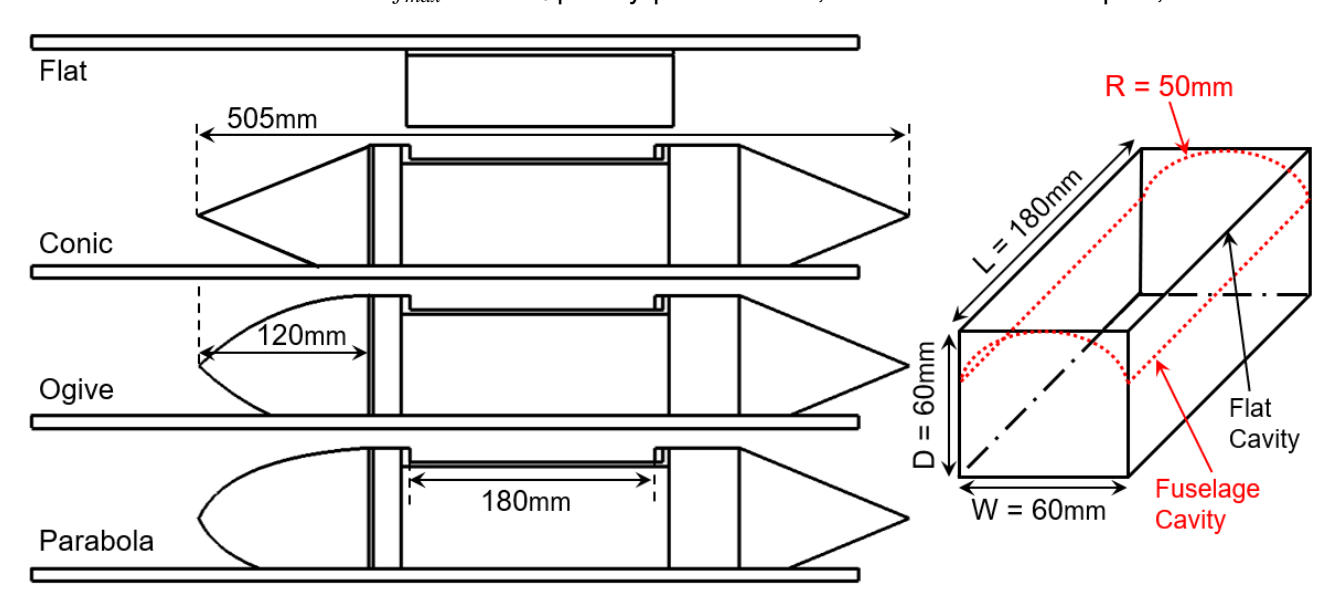


Figure 2 - Schematic of Cavity Model

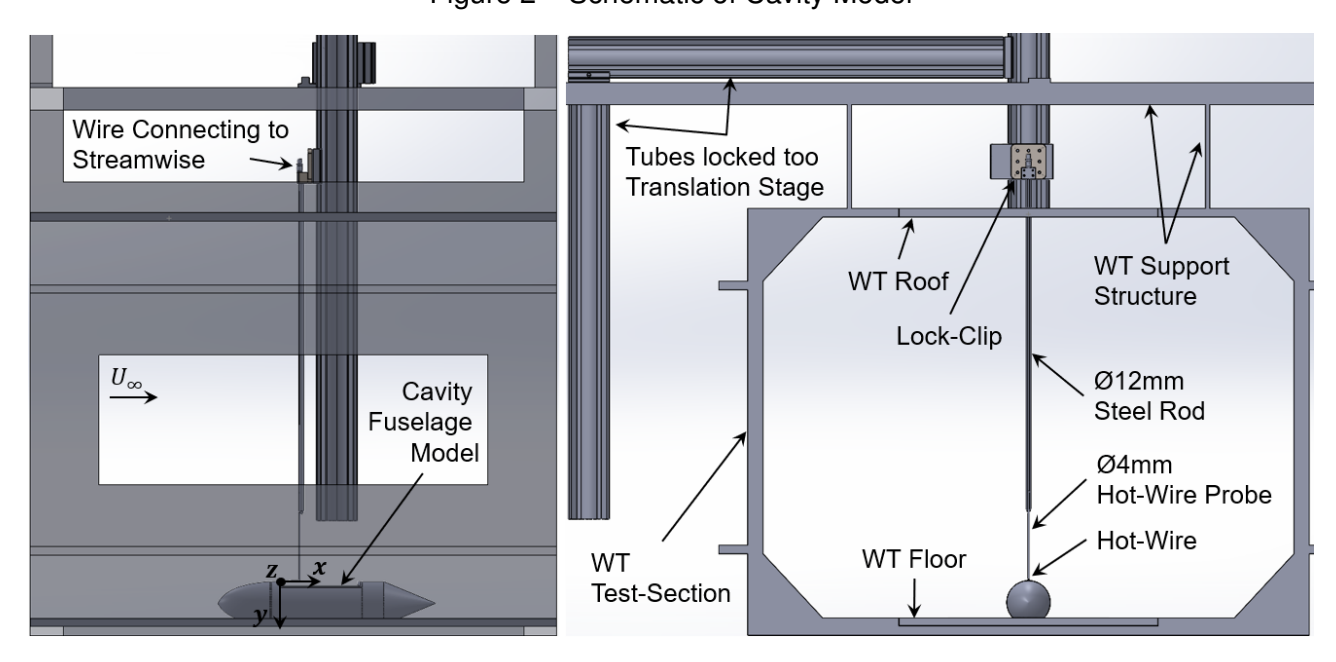


Figure 3 – Hot-Wire Mount Structure Schematic

2.3.3 Data Conversion, Calibration and Uncertainty

A transfer function was used to map CTA voltage output (E) to velocity (u), to enable local velocity (u_i) derivation. The function was established through pre and post calibration, where the sensor

HOT-WIRE ANEMOMETRY OF THE BOUNDARY LAYER PRIOR TO A CAVITY IN RESPONSE TO VARIED

was exposed to known velocities, records response voltage, and fitted data to a curve. The Dantec automatic calibrator was used, simultaneously exposing the sensor to a free-jet, and tracking temperature to update the curve. Equation 1 was the function using a 4th order polynomial curve with constants $C_0 - C_4$, and linearisation error of $< 1\%^{[18]}$. Test velocities were U = 10 - 20m/s, providing a calibration over U = 1 - 30m/s with 50 interval points, based on; $U = 0.1 \cdot U_{min} - 1.5 \cdot U_{max}^{[18]}$. During the test intermediate pitot measurements were also taken to adjust for sensor drift^[19]. Correction for re-scaling, temperature and velocity decomposition is integrated within the Dantec system. Standard ISO uncertainty was used; i.e. a 95% confidence interval, multiplying standard uncertainties U_{y_i} by coverage factor $k_i = 2$, combining contributions U_{y_i} from individual input variance x_i to a total, with output variance $y_i = f(x_i)$, and relative standard uncertainty $u(y_i)$ as a function of input standard deviation in Equation 2. S is sensitivity factor $(\partial y_i/\partial x_i)$ from [18], for total relative expanded uncertainty U_{tot} , with facets prescribed in [18].

$$U_i = C_0 + C_1 \cdot E_i + C_2 \cdot E_i^2 + C_3 \cdot E_i^3 + C_4 \cdot E_i^4$$
(1)

$$u(y_i) = \frac{S}{y_i} \cdot \frac{\Delta x_i}{k_i}$$
 \rightarrow $U_{tot} = 2 \cdot \sqrt{\sum u(y_i)^2}$ (2)

2.4 Unsteady Surface Pressure

2.4.1 Instrumentation and Acquisition

A Scanivalve 4264/64Px Miniature Pressure Scanner (MPS) was used. A script was used to extract data over t = 10s at maximum Scanivalve SR = 800Hz for N = 8000. Internal cavity surfaces were fitted with 258 pressure taps on the fore and aft wall (150), floor (108), and each nose cone had a varying number due to geometric limits: conic (51), ogive (50), and parabola (46). Each tap was a \varnothing 1mm drilled through hole, accommodating a brass tube of outer \varnothing 1mm and inner \varnothing 0.8mm, with a flexible plastic tube of minimum possible length to the pressure scanner at 0.5m, outer \varnothing 2.4mm and inner \varnothing 0.8mm attached with an interference fit at both ends.

2.4.2 Reduction, Uncertainty and Error

Pressure Coefficient C_P was computed with Equation 3; p is tap pressure and $p_\infty, \rho_\infty, U_\infty$ are freestream pressure, density and velocity, respectively. Scanivalve measures the numerator, thus C_P was computed by taking each measurement, and dividing by the denominator of dynamic pressure q_∞ for the run. Time averaged pressure or Root-Mean Square (RMS) was computed using Equation 4. Tube distortion is an error due to variation of oscillatory pressure applied at one end of a tube, when the other end is connected to a pressure sensitive element. An elementary method based on incompressible viscous flow, modified for compressibility to update finite pressure amplitudes, appreciable fluid acceleration, finite length tubes and thermal effects, was derived by Iberall^[20]. This method is used to compute lag and attenuation of a sinusoidal oscillation in a transmission tube. Bergh & Tijdeman ^[21] applied this method with a recursion formula to update dynamic pressure response of a pressure scanner, akin to the present Scanivalve set-up, with a series-connection of j thin tubes and j volumes per Equation 5, relating sinusoidal pressure disturbance in volume V_j to pressure disturbance in preceding V_{j-1} and following volume V_{j+1} , to derive pressure input by successive j = N, N-1, ... 2, 1. All values for the calculation are provided by Scanivalve in [22]

$$C_P = \frac{p - p_{\infty}}{\frac{1}{2} \rho_{\infty} V_{\infty}^2}$$

$$C_{P_{RMS}} = \sqrt{\frac{\sum_{i=1}^N x_i^N}{N}}$$
(4)

$$\frac{p_{j}}{p_{j-1}} = \left[\cosh \left\langle \phi_{j} L_{j} \right\rangle + \frac{V_{v_{j}}}{V_{t_{j}}} \left(\sigma_{j} + \frac{1}{k_{j}} \right) n_{j} \phi_{j} L_{j} \cdot \sinh \left\langle \phi_{j} L_{j} \right\rangle + \frac{V_{t_{j+1}} \phi_{j+1} L_{j} J_{0} \left\langle \alpha_{j} \right\rangle J_{2} \left\langle \alpha_{j+1} \right\rangle}{V_{t_{j}} \phi_{j} L_{j+1} J_{0} \left\langle \alpha_{j+1} \right\rangle J_{2} \left\langle \alpha_{j} \right\rangle} \cdot \frac{\sinh \left\langle \phi_{j} L_{j} \right\rangle}{\sinh \left\langle \phi_{j+1} L_{j+1} \right\rangle} \cdot \left\{ \cosh \left\langle \phi_{j+1} L_{j+1} \right\rangle - \frac{p_{j+1}}{p_{j}} \right\}^{-1} \tag{5}$$

2.5 Experimental Error

- 1. **Sensor Position**: a limit was imposed due to model curvature, probe structure and to avoid breakage. The traverse zero position was held constant relative to the WT axis, this meant sensor position relative to the model slightly varied for each geometry. This is noted in Figure 4 and 5, where the flat and parabola case have more variation, lower on the $Y/\delta_{0.99}$ axis, as the sensor could get closer to the surface without wire or probe bending/breakage. This error is acceptable for present research, to perceive variation in the BL profile in response to U/S geometry, and cavity presence, which remains apparent.
- 2. Airspeed: the WT airspeed controller was due for calibration, thus slight deviation was observed in comparison to hot-wire calibrated recordings in an empty tunnel. Therefore, tunnel airspeed was instead indicated by a HWA taken in the upper section of the tunnel outside the BL, to enable adjustment of indicated airspeed to the test-point, updated with pitot-static tube alignment for accuracy with data recorded to update values.

Note: following wire breakage, a new-wire was calibrated, installed at the same position with resistance re-aligned, and the test redone. Any error due to comparison between wire, is thus accounted for by re-calibration per Equation 1.

3. Results and Discussion

The following results map BL profile U/S of a cavity LE, to correlate cavity response with altered U/S geometry, the impact of a cavity on the BL itself, and how U/S geometry alters cavity response. Figure 4 shows normalised results of mean velocity, the ratio of mean local u_M to free-stream U_{∞} velocity; u/U_{∞} against location in the Y-axis relative to empty WT BL $\delta_{0.99}$ = 39mm. Figure 5 is turbulence intensity (TI) against $Y/\delta_{0.99}$, indicating variation in local velocity u_i over sample time t=60s, at each Y-axis point, as magnitude of relative system stability, or ratio of local velocity root-mean square (RMS) u_{RMS} within samples N, over mean local velocity u_M : $TI(\%) = (u_{RMS}/u_M)$.

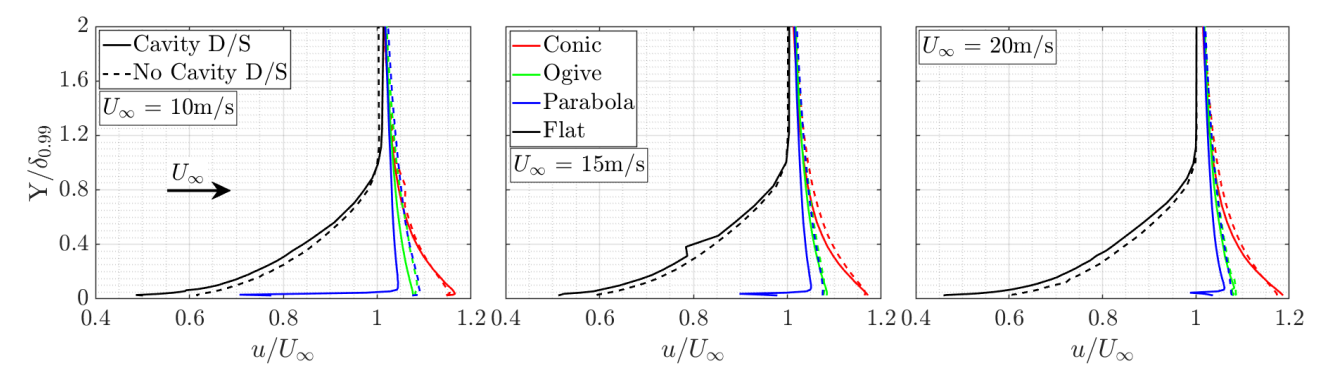


Figure 4 – HWA BL Mean Velocity (U_M ,m/s) at 10, 15, 20 m/s

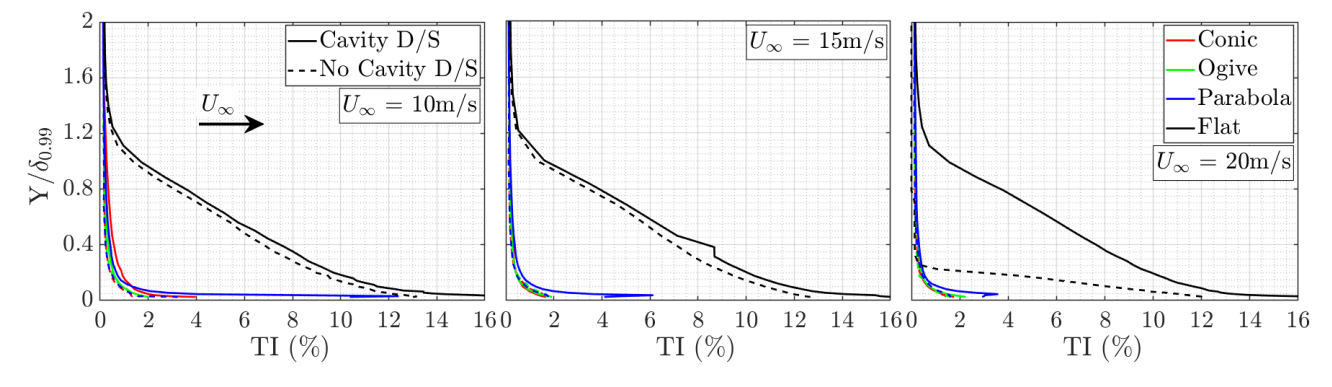


Figure 5 – HWA BL Turbulence Intensity (TI,%) for Tunnel Setting at 10, 15, 20 m/s

In Figure 4 and 5, when the cavity is not present, it's apparent U/S geometry alters the BL profile shape and magnitude with regard to u/U_{∞} and TI, especially between the flat baseline case and nose shapes. The flat case, exhibits a standard flat-plate Newtonian BL profile, with reduction in local velocity relative to the free-stream within the BL, until the disturbance thickness $\delta_{0.99} \approx 39mm$. However, the nose-cones which were elevated out of the tunnel BL δ , experience free-stream velocity U_{∞} impingement at the cone LE. In this case, the flow is accelerated along the positive gradient of the nose cone D/S with flow retardation towards the main body of the model^[23]. This causes a relative increase in local velocity u at the cone TE and thus cavity LE compared to the U_{∞} outside the BL, in line with flow physics of Falkner-Skan's^[24] for wedge flow, adapted from Prandtl BL theory^[23].

Similar trends are present for almost all U_{∞} , aside from the parabola case in presence of a cavity, where TI reduces proportionally with U_{∞} per Figure 5, and u/u_{∞} increases with airspeed U_{∞} per 4. The latter is representative of a relative increase in flow development over the nose cone with increasing airspeed, toward ideal flow acceleration per [24], compared to a very turbulent unstable profile at $U_{\infty}=10m/s$, where viscosity is more abundant. At $U_{\infty}=15m/s$, a blip is perceived at $Y/\delta_{0.99}\approx0.25$. This is an accidental repetition of the prior $Y/\delta_{0.99}$ point due to similarity in the x-axis value, also observable in Figure 4 and 5 is experimental error (2) per Section 2.5 In this case, slightly more variation is perceived for the flat and parabola cases, as the sensor could get closer to the surface.

In all cases, a consistent increase in plot curvature magnitude and gradient is observed between cavity presence and cavity absence. This indicates the cavity increases local viscous effects within the U/S BL, slightly thickening the BL profile, thus increasing turbulence and reducing local velocity within the profile. The ogive case remains consistent between airspeed, and also in the presence of the cavity, suggesting a potentially ideal geometry for reducing the increased viscous effects of cavity presence. However, it's possible the effect may become abundant with increasing airspeed. Characterisation of cavity effect on U/S BL flow, is in progress, using spectral analysis of a larger, more discrete data set of external and internal HWA and USP. To parameterise the U/S BL and viscosity due to cavity presence, and thus D/S effects on the cavity itself for optimised spectral prediction of cavity response including feedback effects.

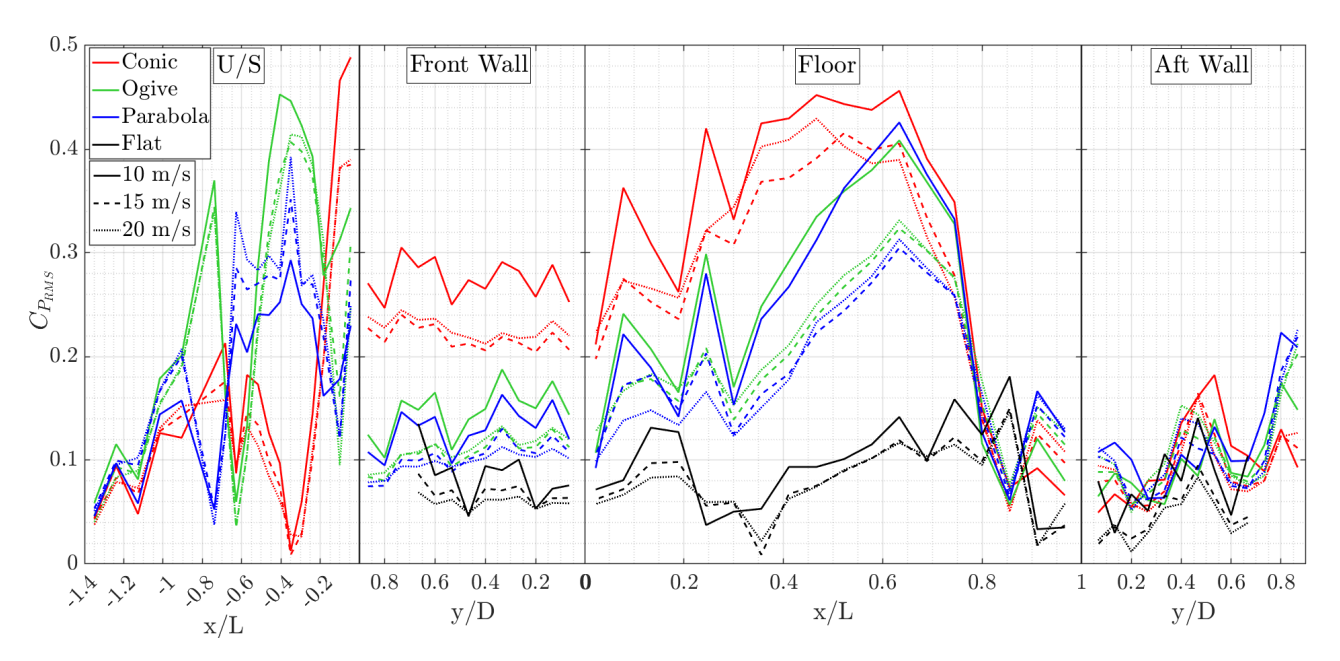


Figure 6 - Cavity Surface Response: Coefficient of Pressure Root-Mean Square

Figure 6 is a plot of $C_{P_{RMS}}$, over the U/S and internal surfaces of the cavity, for each U_{∞} and U/S geometry. Along with Figures 4 and 5, Figure 6 highlights a clear shift in USP response U/S and internal to the cavity, due to change in U/S geometry. The conic nose produces more unsteadiness on the internal surfaces, especially fore wall and floor, this effect increasing with U_{∞} . It must be noted at 10m/s, WT flow stability in the test section isn't uniform so the data isn't ideal for comparison. How-

ever, it was included to show the impact of a more intense fluctuating flow on the relative magnitude of change for cavity response. As U_{∞} increases however, flow is known to straighten in the WT U/S. This causes an initial reduction in pressure fluctuation intensity. Though a proportional increase in $C_{P_{RMS}}$ is then observed in the cavity with U_{∞} . This is less apparent for the flat case, along the floor of the cavity, as the U/S BL profile had a high level of TI, which would filter any large changes within this regime. However, the lower levels of TI, but higher level of flow acceleration over the nose cones, has caused relative uniformity in the flow, resulting in a more periodic cavity response. This is possibly due to less flow separation, enabling larger and more periodic shedding of vortices at the LE, versus noisy random bursts in the flat case, due to the thick turbulent BL.[7; 8; 15].

4. Conclusions

Each LE BL profile, generated though several fuselage geometries, impacted cavity response. The conic shape had a notable impact on the cavity, consistent with the highest level of flow acceleration U/S. This led to a LE separation with a higher velocity and resulted in a more unsteady response, with a 10% increase in unsteady RMS fluctuations on the cavity floor, potentially due to a slight reduction of TI. Here it is thought that the accelerated flow reduced local viscous effects[24], enabling higher periodicity in LE shed vortices[7], hence higher $C_{P_{RMS}}$. Especially considering comparatively high TI and BL δ of the flat case, this BL characteristic appeared to give a less intense response, overall indicating the impact of BL profiles on cavity response.

The cavity presence also impacts BL development, especially the viscosity gradient, expected to be a result of flow feedback within the cavity, which can be isolated when observing the BL in the absence of a cavity. Further work will categorise spectra response via DMD, spectral and statistical analysis, in alignment with the cavity and BL energy. This future work to will derive a mathematical correlation between the two quantities, for integration into cavity flow prediction models.

Contact Author Email Address

The contact author please email caroline.hamiltonsmith@sydney.edu.au.

Copyright Statement

The authors confirm that they, and/or their company or organization, hold copyright on all of the original material included in this paper. The authors also confirm that they have obtained permission, from the copyright holder of any third party material included in this paper, to publish it as part of their paper. The authors confirm that they give permission, or have obtained permission from the copyright holder of this paper, for the publication and distribution of this paper as part of the ICAS proceedings or as individual off-prints from the proceedings.

Acknowledgements

Advanced Piezoelectric Materials and Applications Program, through DMTC Limited (Australia), and funded by Defence under the Next Generation Technologies Fund, which is now administered through the Advanced Strategic Capabilities Accelerator. The authors have prepared this paper in accordance with the intellectual property rights granted by a DMTC Project Agreement

Zonta International Amelia Earhart Fellowship, est. 1938 in honor of famed pilot Amelia Earhart.

References

- [1] V. Sarohia, Experimental Investigation of Oscillations in Flows over Shallow Cavities, AIAA Journal 15 (7) (1977) 984–991. doi:10.2514/3.60739.
- [2] J. Scheiman, Acoustic Measurements of a Large Cavity in a Wind Tunnel, Tech. Rep. NASA-TM-78658, NASA Langley Research Center, Hampton, Virginia, USA (May. 1978). doi:https://ntrs.nasa.gov/citations/19780017887.
- [3] J. Milbank, Investigation of Fluid-Dynamic Cavity Oscillations and the Effects of Flow Angle in an Automotive Context using an Open-Jet Wind Tunnel, Ph.D. thesis, School of Aerospace, Mechanical and Manufacturing Engineering, RMIT University, Melbourne, VIC, Australia (Aug. 2004).

- [4] S. Grace, W. Dewar, D. Wroblewski, Experimental Investigation of the Flow Characteristics within a Shallow Wall Cavity for both Laminar and Turbulent Upstream Boundary Layers, Experiments in Fluids 36 (5) (2004) 728–740. doi:10.1007/s00348-003-0761-3.
- [5] K. Chang, G. Constantunescu, S.-O. Park, Analysis of the Flow and Mass Transfer Process for the Incompressible Flow Past an Open Cavity with a Laminar and Fully Turbulent incoming Boundary Layer, Journal of Fluid Mechanics 561 (2006) 113–145. doi:10.1017/S0022112006000735.
- [6] C. Haigermoser, L. Vesely, M. Novara, M. Onorato, Visualizations of the Flow Inside an Open Cavity at Medium range Reynolds Numbers, Physics of Fluid 20 (10) (2008) 105101. doi: 10.1063/1.2990043.
- [7] K. Karamcheti, Acoustic Radiation from Two-Dimensional Rectangular Cutouts in Aerodynamic Surfaces, Tech. Rep. NACA-TN-3487, NACA, Washington, D.C. USA. (Aug. 1955). doi:https://ntrs.nasa.gov/citations/19930084329.
- [8] A. Roshko, Some Measurements of Flow in Rectangular Cutout, Tech. Rep. NACA-TN-3488, National Advisory Committee for Aeronautics (NACA), Washington, D.C. USA. (Aug. 1955). doi:https://ntrs.nasa.gov/citations/19930084332.
- [9] A. Charwat, J. Roos, F. Dewey, Jr, J. Hitz, An Investigation of Separated Flows Part 1: The Pressure Field, Journal of Aerospace Sciences 28 (6) (1961) 457–470. doi:10.2514/8. 9037.
- [10] P. Block, H. Heller, Measurements of Far-Field Sound Generation from a Flow-Excited Cavity, Tech. Rep. NASA-TM-X-3292, NASA Langley Research Center, Hampton, VA, USA (Dec. 1975). doi:https://ntrs.nasa.gov/citations/19760006791.
- [11] K. Ahuja, J. Mendoza, Effects of Cavity Dimensions, Boundary Layer and Temperature on Cavity Noise with Emphasis on Benchmark Data to Validate Computational Aeroacoustic Codes, Tech. Rep. NASA Contractor Report 4653, Georgia Institute of Technology, Atlanta, GA, USA (Apr. 1995).
- [12] T. Colonius, A. Basu, C. Rowley, Numerical Investigation of the Flow Past a Cavity, in: 5th AIAA/CEAS Aeroacoustics Conference and Exhibit, AIAA, Bellevue, WA, USA, 1999, pp. AIAA–99–1912. doi:10.2514/6.1999-1912.
- [13] C. Rowley, I. Mezić, S. Bagheri, . Schlatter, P, D. Henningson, Spectral Analysis of Nonlinear Flows, Journal of Fluid Mechanics 641 (2009) 115–127. doi:10.1017/S0022112009992059.
- [14] A. Seena, H. Sung, Dynamic Mode Decomposition of Turbulent Cavity Flows for Self-Sustained Oscillations, International Journal of Heat and Fluid Flow 32 (2011) 1098–1110. doi:10.1016/j.ijheatfluidflow.2011.09.008.
- [15] M. Gharib, A. Roshko, The Effect of Flow Oscillations on Cavity Drag, Journal of Fluid Mechanics 177 (4) (1987) 501–530. doi:10.1017/S002211208700106X.
- [16] K. Karamcheti, Sound Radiated from Surface Cutouts in High-Speed Flows, Ph.D. thesis, Caltech, Pasadena, CA, USA (1956). doi:https://thesis.library.caltech.edu/1129/.
- [17] W. Kang, S. Lee, H. Sung, Self-Sustained Oscillations of Turbulent Flows over an Open Cavity, Experiments in Fluids 45 (2008) 693–709. doi:10.1007/s00348-008-0510-8.
- [18] F. Jørgensen, How to Measure Turbulence with Hot-Wire Anemometers, Tech. Rep. 9040U6152, Dantec Dynamiucs A/S, P.O. Box 121, Tonsbakken 16-18, DK-2740 Skovlunde, Denmark (Jun. 2004).

- [19] K. Talluru, V. Kulandaivelu, N. Hutchins, I. Marusic, A Calibration Technique to Correct Sensor Drift Issues in Hot-Wire Anemometry, Measurement Science and Technology 25 (105304) (Jun. 2014). doi:10.1088/0957-0233/25/10/105304.
- [20] A. Iberall, Attenuation of Oscillatory Pressures in Instrument Lines, Part of the Journal of Research of the National Bureau of Standards 45 (RP2115) (1950) 85–108. doi:10.6028/JRES.045.008.
- [21] H. Bergh, H. Tijdeman, Theoretical and Experimental Results for the Dynamic Response of Pressure Measuring System, Tech. Rep. NLR-TR F.238, National Aero- and Astronautical Research Institute, Amsterdamn, NETH (Jan. 1965). doi:10.13140/2.1.4790.1123.
- [22] R. Pemberton, An Overview of Dynamic Pressure Measurement Considerations, Tech. rep., Scanivalve Corporation, Liberty Lake, WA, USA (Mar. 2010).
- [23] L. Prandtl, Über Flüssigkeitsbewegung bei sehr kleiner Reibung, in: Verhandlungen des III: Internationalen Mathematiker Kongresses, B. G. Teubner, Leipzig, Heidelberg, GER, 1904, pp. 485–491.
- [24] V. Falkner, S. Skan, Some Approximate Solutions of the Boundary Layer Equations., Philosophical Magazine 12 (80) (1931) 865–896. doi:10.1080/14786443109461870.

Appendix: Wind Tunnel Test Matrix

Table 1 – Wind Tunnel Test Matrix of Ambient Conditions

Nose	Cavity	$U_{\infty}(m/s)$	ρ_{∞} (kg/m ³)	μ _∞ (Pa.s)	T_{∞} (C $^{\circ}$)	P_{∞} (kPa)	Re. No.
Conic	Yes	10	1.16	1.86E-05	29.6	100.6	7.6E+05
Conic	Yes	15	1.16	1.86E-05	29.6	100.6	1.1E+06
Conic	Yes	20	1.18	1.84E-05	25.5	101.1	1.6E+06
Ogive	Yes	10	1.18	1.84E-05	25.8	101.0	7.8E+05
Ogive	Yes	15	1.18	1.84E-05	25.9	101.0	1.2E+06
Ogive	Yes	20	1.17	1.84E-05	26.1	100.8	1.6E+06
Parabola	Yes	10	1.20	1.83E-05	23.7	102.6	8.0E+05
Parabola	Yes	15	1.20	1.83E-05	23.9	102.6	1.2E+06
Parabola	Yes	20	1.20	1.83E-05	24.3	102.6	1.6E+06
Flat	Yes	10	1.15	1.86E-05	30.6	100.4	7.5E+05
Flat	Yes	15	1.15	1.86E-05	29.8	100.2	1.1E+06
Flat	Yes	20	1.15	1.86E-05	30.5	100.2	1.5E+06
Conic	No	10	1.16	1.87E-05	31.8	101.5	7.6E+05
Conic	No	15	1.16	1.86E-05	30.8	101.5	1.1E+06
Conic	No	20	1.16	1.86E-05	30.7	101.4	1.5E+06
Ogive	No	10	1.17	1.86E-05	30.0	102.0	7.7E+05
Ogive	No	15	1.17	1.86E-05	29.8	102.0	1.2E+06
Ogive	No	20	1.17	1.86E-05	29.7	102.0	1.5E+06
Parabola	No	10	1.17	1.86E-05	30.7	102.0	7.6E+05
Parabola	No	15	1.17	1.87E-05	31.0	101.9	1.1E+06
Parabola	No	20	1.17	1.87E-05	31.2	102.0	1.5E+06
Flat	No	10	1.16	1.86E-05	29.6	100.6	7.6E+05
Flat	No	15	1.15	1.86E-05	30.5	100.6	1.1E+06
Flat	No	20	1.15	1.87E-05	30.9	100.6	1.5E+06